Photosynth Res (2011) 108:215–224
DOI 10.1007/s11120-011-9682-9

REGULAR PAPER

Photosynthetic energy storage efficiency in *Chlamydomonas reinhardtii*, based on microsecond photoacoustics

Chengyi Yan · Oscar Schofield · Zvy Dubinsky · David Mauzerall · Paul G. Falkowski · Maxim Y. Gorbunov

Received: 31 March 2011 / Accepted: 15 August 2011 / Published online: 6 September 2011
© Springer Science+Business Media B.V. 2011

Abstract Using a novel, pulsed micro-second time-resolved photoacoustic (PA) instrument, we measured thermal dissipation and energy storage (ES) in the intact cells of wild type (WT) *Chlamydomonas reinhardtii*, and mutants lacking either PSI or PSII reaction centers (RCs). On this time scale, the kinetic contributions of the thermal expansion component due to heat dissipation of absorbed energy and the negative volume change due to electrostriction induced by charge separation in each of the photosystems could be readily distinguished. Kinetic analysis revealed that PSI and PSII RCs exhibit strikingly different PA signals where PSI is characterized by a strong electrostriction signal and a weak thermal expansion component while PSII has a small electrostriction component and large thermal expansion. The calculated ES efficiencies at $\sim$10 μs were estimated to be 80 ± 5 and 50 ± 13% for PSII-deficient mutants and PSI-deficient mutants, respectively, and 67 ± 2% for WT. The overall ES efficiency was positively correlated with the ratio of PSI to PSI + PSII. Our results suggest that the shallow excitonic trap in PSII limits the efficiency of ES as a result of an evolutionary frozen metabolic framework of two photosystems in all oxygenic photoautotrophs.

C. Yan · O. Schofield · P. G. Falkowski · M. Y. Gorbunov (✉)
Environmental Biophysics and Molecular Ecology Program, Institute of Marine and Coastal Sciences, Rutgers, The State University of New Jersey, New Brunswick, NJ 08901, USA
e-mail: gorbunov@marine.rutgers.edu

Z. Dubinsky
Department of Life Sciences, Bar Ilan University, Ramat Gan, Israel

D. Mauzerall
Rockefeller University, New York, NY 10065, USA

Keywords Energy storage efficiency · Photoacoustics · Photosystem I · Photosystem II · *Chlamydomonas reinhardtii*

Introduction

The photoacoustic (PA) effect, discovered by Bell (1880), measures the conversion light energy to acoustic waves. The PA technique has been applied in many fields, such as biomedical imaging (Xu and Wang 2006), tomography (Paltauf et al. 2007), and has also been used to directly assess the overall thermal dissipation in PSII and PSI as a result of heat loss in the photosynthetic reactions (Callis et al. 1972; Cahen et al. 1978; Malkin and Cahen 1979; Feitelson and Mauzerall 1993; Malkin and Canaani 1994; Mauzerall et al. 1995a, b, 1998; Malkin 1996). In spite of the seemingly straightforward physics, practical applications of the PA technique in photosynthesis research and ecophysiology remain limited by the complexity of the intermediate biophysical processes in photochemical energy transduction, the cost of existing laser-based PA systems, and low sensitivity (Fork and Herbert 1993; Malkin and Canaani 1994; Herbert et al. 2000; Delosme 2003).

Absorption and conversion of light energy in photosynthetic reactions may lead to negative volume change due to contraction of the reaction centers (RCs) by electrostatic force induced by charge separation. This electrostriction effect is superimposed on the thermal expansion pressure wave (Braslavsky and Heibel 1992; McClean et al. 1998; Wegewijs et al. 1998; Borsarelli and Braslavsky 1998, 1999; Losi et al. 1999; Herbert et al. 2000; Delosme 2003). Hence, the quantitative interpretation of the PA signals requires the knowledge of the thermal

expansion coefficient of the medium. Although, most of the PA signals from a suspension of algae are caused by thermal expansion of water (Braslavsky and Heibel 1992; Fork and Herbert 1993; Herbert et al. 2000; Delosme 2003), the cellular constituents (lipids and proteins) have different thermal expansion properties (Boichenko et al. 2001), which further complicates the interpretation of PA signals.

Thermal dissipation and electrostriction can suddenly expand or shrink the surrounding medium, inducing pressure waves that can be detected by a piezoelectric transducer in an aqueous phase (Brumfeld et al. 1999). These two types of PA signals can be distinguished by comparing the measurements at different temperature (Callis et al. 1972; Arata and Parson 1981; Delosme et al. 1994; Edens et al. 2000). Here, we developed a compact PA system with excitation by short flashes from light-emitting diodes (LEDs) and PA wave recording by a fast-response resonance piezoelectric detector, which achieves microsecond time resolution. The introduction of LEDs instead of previously used pulsed lasers allowed us, for the first time, to build a compact PA instrument that is particularly convenient for both laboratory and field studies. The PA system also allows measurements of fast induction phenomena, including S states of the oxygen evolving complex in leaf tissue (Canaani et al. 1988; Mauzerall 1990), the earliest steps of photosynthetic electron transport (Delosme 1998; Edens et al. 2000; Boichenko et al. 2001; Hou et al. 2001a, b), and energy storage (ES) in PSI or PSII (i.e., the ratio of the energy stored in the photochemical products to the absorbed energy; Malkin and Canaani 1994; Boichenko et al. 2001; Hou et al. 2001a, b). Previous PA studies showed that the ES efficiency in PSI on the microsecond time scale was >70% in both the isolated particles (Nitsch et al. 1988) and intact cyanobacterial cells (Mullineaux et al. 1991; Bruce and Salehian 1992). Pulsed PA systems also have been used to measure ES during steady state photosynthesis in intact cells and leaves (Kolbowski et al. 1990; Boichenko et al. 2001; Hou et al. 2001a, b).

Using our newly developed PA system, we present the kinetic patterns for the individual photosystems in vivo in the green alga, *Chlamydomonas reinhardtii* at microsecond time resolution. Our approach allows kinetic separation of the thermal and electrostrictive components of the photochemical reactions and hence the contributions of each to the ES efficiencies of each RC. The data suggest fundamental biophysical limitations in PSII, resulting from the energetically shallow excitonic trap, constrain photochemical energy conversion efficiency in oxygenic photosynthesis.

Materials and methods

Culture growth condition

All cultures were provided by the *Chlamydomonas* Center at Duke University. In addition to the wild type (WT) clone, CC-125, we grew the PSI-deficient mutants CC-4134 and CC-1042, the PSII-deficient mutants CC-4151 and CC-1051 in 500 ml flasks containing liquid Sueoka's high salt medium with acetate addition (Sueoka 1960) at pH 7.0 and 25°C under a 12/12 h light/dark cycle supplied by cool-white fluorescent tubes. For optimal growth conditions, the WT was cultivated at 200 μmol quanta m^{-2} s^{-1} while the mutants were kept at 50 μmol quanta m^{-2} s^{-1}. All cultures were bubbled with filtered CO_2-enriched air (5% CO_2). Growth rates were determined by direct cell counts. During the light part of the cycle, algal cells were harvested at the late exponential phase (about 8.0×10^6 cells ml^{-1}) by centrifugation at 2000×*g* for 5 min and washed and resuspended in media to achieve the final concentration of 1.5×10^6 cells ml^{-1} for the experiments.

Low-temperature fluorescence spectroscopy

Fluorescence emission spectra were measured at 77 K in dark-adapted cells. Triplicate, quantum corrected spectra were obtained with an SLM/Aminco 4800 spectrofluorometer (Rochester, NY) using an internal standard with an excitation wavelength of 435 nm. Quantum corrected emission spectra were deconvoluted in the wavenumber domain, assuming a Gaussian distribution of the excited states (Mimuro et al. 1982).

PA apparatus and measurements

PA kinetic measurements were obtained with a custom built, LED-based instrument (Fig. 1). The instrument incorporates a suite of ultra-bright LEDs (Lumileds Co.) as a source of microsecond pulses to induce the PA signal. The LEDs emit flashes of red light at 640 nm wavelength with a 30 nm half bandwidth. Pulse duration is adjustable from 1 to 25 μs. The optimal flash duration was selected at 8 μs to match the oscillation semi-period of the piezo-acoustic resonance-based detector.

A set of continuous-wave ultra-bright blue LEDs (470 nm wavelength, 30 nm half bandwidth) was incorporated into the optical scheme to provide a source of saturating illumination. The intensity of the saturating light was adjusted to ca. 4,000 μmol quanta cm^{-2} s^{-1} to ensure closure of RCs. The excitation from both red and blue LEDs was focused into the 40 mm^2 spot in the sample chamber. The sample chamber was a 50-mm diameter

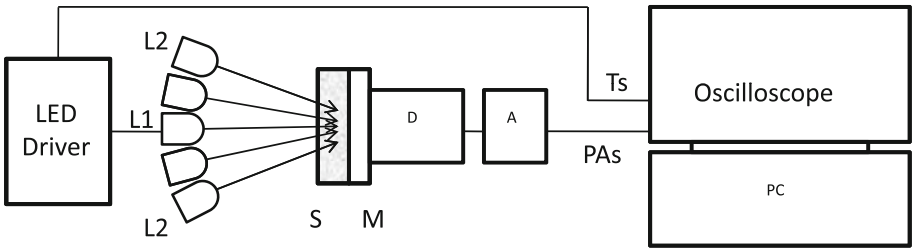

Fig. 1 Schematic diagram of the photoacoustic system: *L1* pulsed LED flasher; *L2* continuous-wave LEDs, *S* temperature-controlled sample chamber, *M* dielectric mirror, *D* piezo-electric detector, *A* charge sensitive amplifier, *Ts* trigger signal, and *PAs* PA signal

quartz cuvette with 1 cm optical path. A high-reflective dielectric mirror (99.5% reflection between 600 and 700 nm, Newport) was installed behind the cuvette followed by a custom-built microphone detector that contains a 5 mm ceramic Lead Zirconite Titanates piezo-disk in a stainless steel holder.

The pulsed signals from the piezoelectric detector were amplified by a charge sensitive amplifier (Amptek A-203), averaged over a preset number of pulses (ranging from 200 to 500, depending on the signal) using a digital oscilloscope (Tektronix TDS 544A or similar), and stored.

In order to avoid saturation effects, weak measuring pulses (equivalent to <0.1 hits per RC per pulse) were applied to generate PA signals. The pulse intensity (in units of hits per RC) was estimated by titrating the PA signals versus the pulse energy and approximating the resulting profile with a one-hit Poisson distribution, as described by Charlebois and Mauzerall (1999). While measuring PA signals for open RCs, we applied the measuring pulses following at low repetition rate (<5 Hz). While measuring PA signals for closed centers, the repetition rate was increased to ~100 Hz to avoid a prolonged exposure of the sample to strong saturating light. Three to five replicates were measured for each sample.

Results

Low-temperature fluorescence spectra

In green algae, the spectrum of fluorescence emission at 77 K reflects the relative abundance of PSII and PSI. Two fluorescence emission bands, one at ~685 nm and second at ~695 nm, are derived from PSII core antenna pigment proteins, CP43 and CP47, respectively (Krause and Weis 1991), whereas a longer wavelength, broad band between 710 and 735, is ascribed to PSI antenna pigments (Murata et al. 1966). In *C. reinhardtii* grown under different light regimes, the 77 K fluorescence ratios (F_{PSI}/F_{PSII}) correlate closely with photosystem stoichiometries (PSI/PSII) and have the following linear relationships: PSI/PSII (mol/mol) = 0.87 × F_{PSI}/F_{PSII} or PSI/(PSI + PSII) (mol/mol) = 0.92 × $F_{PSI}/(F_{PSI} + F_{PSII})$ (Murakami1997).

Analytical decomposition of the 77 K fluorescence emission spectra (Figs. 2, 3) revealed the presence of these components in the WT cells (Fig. 2) but the lack of the respective RCs in the 4 mutants (Fig. 3). The characteristics of the component bands and PSI/PSII stoichiometries, based on integrated areas under the respective emission bands are summarized in Table 1. These results reveal that

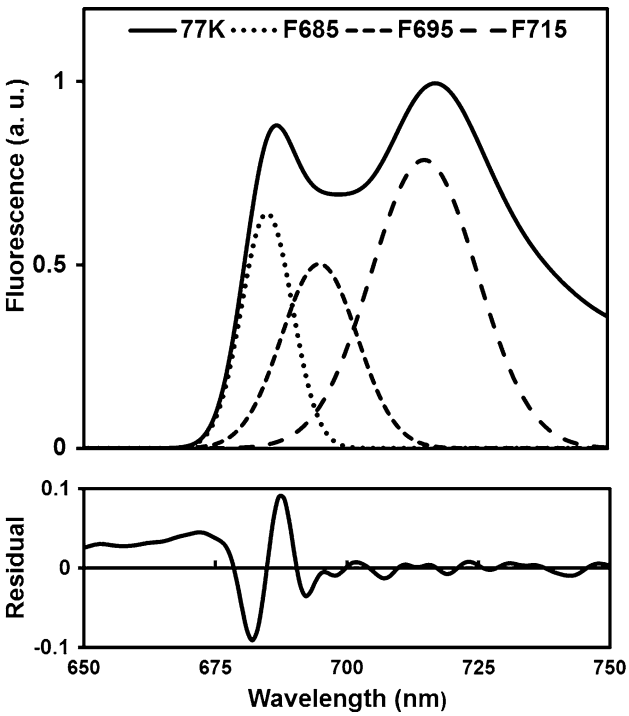

Fig. 2 Deconvolution analysis of 77 K fluorescence emission spectra of wild type of *C. reinhardtii*, fitted to Gaussian components. Fluorescence emission spectra were measured with the excitation at 435 nm. The original 77 K spectrum was pre-smoothed at 2% level using a Gaussian convolution method and then deconvoluted using software PeakFit v4. The three fluorescence bands, corresponding to the excitation at 685, 695, and 715 nm, respectively, are shown. All the fluorescence bands between 710 and 735 nm were integrated into one 715 nm band, representing the PSI component. The *bottom panel* shows the residuals between the measured spectra and the best fit. The spectrum was normalized to the maximal activities

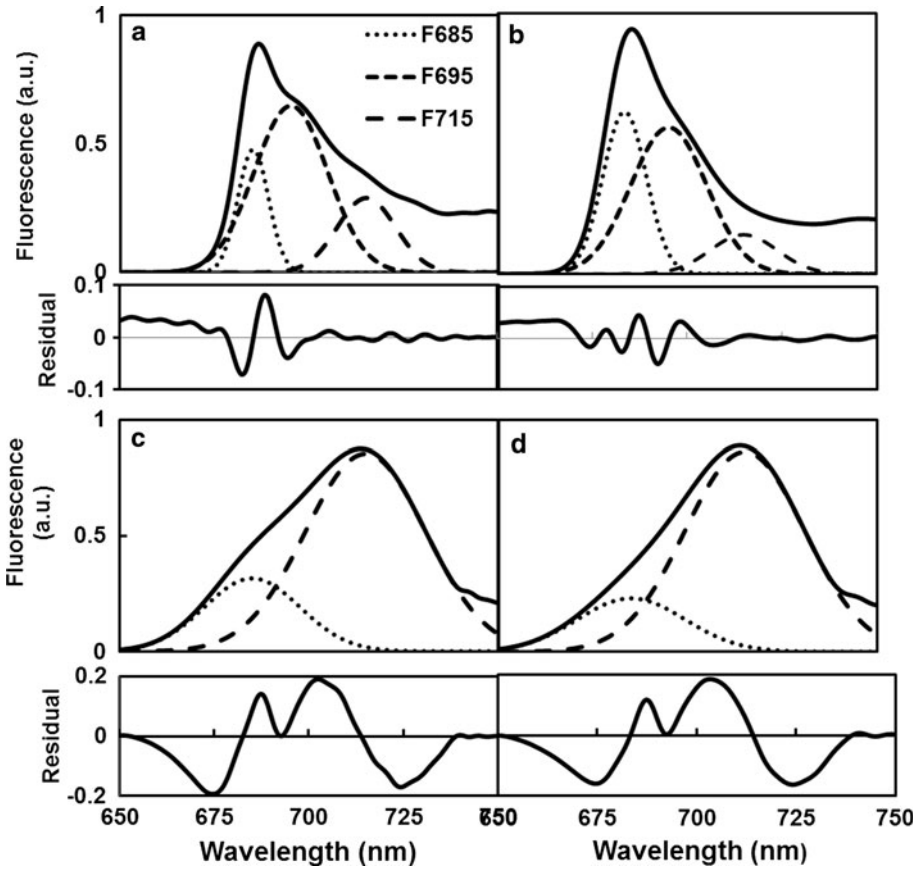

Fig. 3 Deconvolution analysis of 77 K fluorescence emission spectra of *C. reinhardtii* mutants, fitted to Gaussian components. **a** CC-4134; **b** CC-1042; **c** CC-4151; and **d** CC-1051. Fluorescence emission spectra were measured with the excitation at 435 nm. The original 77 K spectrum was pre-smoothed at 2% level using Gauss convolution method and then deconvoluted using software PeakFit v4. Only three florescence bands corresponding to the excitation at 685, 695, and 715 nm, respectively, are showed while others were removed. All the fluorescence bands between 710 and 735 nm were integrated into one 715 nm band, representing the PSI component. The *bottom panel* showed the residuals between the measured spectra and the best fit

the two PSII-deficient mutants lack the 695 nm component (Fig. 3c and d; Table 1), although a low amount of the 685 nm component was retained. For different types of cells, the emission peaks of PSI fluorescence emission varied between 710 and 718 nm (718, 715, 717, and 710 nm), but the emission peaks of PSII are fairly constant at approximately 685 and 695 nm, respectively. As shown in Figs. 2, 3 and in Table 1, we integrated the fluorescence bands between 710 and 735 nm into one 715 nm band, representing the PSI component. These results revealed that the mutants contain small quantities of the complementary RCs, but the ratios of PSI/PSII differed markedly from the WT (Table 1). Our calculated PSI/PSII ratio of 1.03 for the WT is in good agreement with the previously published values of 1.16 (Polle et al. 2000) and 0.87–0.98 (Murakami et al. 1997).

Kinetics of the PA signals

In this study, the PA signals were attributed to either thermal expansion and/or electrostriction since there is no O_2 evolution in $\sim$10 μs time window. The electrostriction produces a negative volume change, resulting in 180° phase shift in the PA signal compared to the thermal expansion. We used black ink as an external calorimetric reference, which was adjusted to the same optical density as the sample at a given wavelength in the same buffer medium. The ink dissipates all absorbed photons into heat much faster than the PA resolution time scale (Boichenko et al. 2001). We also utilized the internal calorimetric reference of the algal sample upon exposure to saturate background illumination when the heat dissipation was maximum due to fully closed RCs (Boichenko et al. 2001). The separation of thermal expansion component relies on PA measurements at 4°C (e.g., the maximum density of liquid water), where thermal expansion signal is abolished since the thermal expansion of water is zero at 4°C (Callis et al. 1972; Arata and Parson 1981; Delosme et al. 1994; Edens et al. 2000) while electrostriction remains unaltered (Malkin and Canaani 1994). The contribution of electrostriction varies dramatically with the state of RCs, being maximal when RCs are open, and minimal to zero in fully closed RCs, (e.g., under saturating background illumination) (Hou et al. 2001a, b). Therefore, the PA spectrum will only contain the thermal expansion signal of the total absorbed light under saturating background illumination. The combination of the measurements at different temperatures and different background illumination permits separation of the PA profiles into the thermal expansion and electrostriction components.

Table 1 Characteristics of the component bands and PSI/PSII stoichiometries originated from PSII (F_{685} and F_{695}) and PSI (F_{685}) of 77 K fluorescence emission spectra

Culture	F_{PSII}		F_{PSI}	F_{PSI}/F^{b}_{PSII}	$F_{PSI}/(F_{PSI} + F_{PSII})^{c}$	PSI/PSII[d]	PSI/(PSI + PSII)[e]
	F^{a}_{685}	F^{a}_{695}	F^{a}_{715}				
WT	7.77	9.11	20.00	1.18	0.54	1.03	0.50
CC-4134	4.87	15.79	5.63	0.27	0.21	0.23	0.19
CC-1042	8.95	14.15	3.35	0.15	0.13	0.13	0.12
CC-4151	10.00	–	34.06	3.40	0.77	2.96	0.71
CC-1051	8.25	–	34.21	4.15	0.81	3.61	0.75

[a] All fluorescence values were calculated by measuring the area enclosed by the fluorescence spectra at each excitation wavelength (685, 695, and 715 nm, respectively)

[b] The ratio of $F_{PSI}/F_{PSII}$was calculated as $F_{715}/(F_{685} + F_{695})$

[c] The ratio of $F_{PSI}/(F_{PSI} + F_{PSII})$ was calculated as $F_{715}/(F_{685} + F_{695} + F_{715})$

[d] The ratio of PSI/PSII was calculated as PSI/PSII = $0.87 \times F_{PSI}/F_{PSII}$ (Murakami 1997), on the assumption that each PSI contains the fluorescence bands F_{715} and each PSII contains two fluorescence bands, F_{685} and F_{695}

[e] The ratio of PSI/(PSI + PSII) was calculated as PSI/(PSI + PSII) = $0.92 \times F_{PSI}/(F_{PSI} + F_{PSII})$ (Murakami 1997), on the assumption that each PSI contains the fluorescence bands F_{715} and each PSII contains two fluorescence bands, F_{685} and F_{695}. All values were relative ($r^2 > 0.90$)

When the RCs were closed by saturating light, a positive phase PA signal was observed at 25°C (Fig. 4, curve 1). This signal had the same shape and phase as the reference signal from ink (Fig. 4, curve 5). In contrast, the signal of open RCs (Fig. 4, curve 3) was a phase shifted by 180°, which is indicative of the overall negative volume change and, hence, the dominance of electrostriction. A negative PA wave with larger amplitude was created in the absence of background light at 4°C (Fig. 4, curve 2) because of the absence of the thermal signal. Upon the closure of the RCs with saturating background light at 4°C, a weak wave was observed (Fig. 4, curve 4). No PA signal (Fig. 4, curve 6) was observed from carbon ink at 4°C.

In intact cells, the thermal expansion coefficients of cellular constituents differ from those of the surrounding water. This may lead to a residual PA signal measured under continuous saturating light at 4°C (Fig. 4, curve 4) called the "cellular artifact" (Boichenko et al. 2001). We corrected all three PA profiles by subtracting this "artifact" (see below for details) and then smoothed them with Savitzky–Golay filter function in the Origin 6.0 program. Typical, corrected PA profiles are shown in Fig. 5. The PA profiles of PSI-deficient mutants (CC-4134 and CC-1042) have different patterns than PSII-deficient mutants (CC-4151 and CC-1051). The latter were similar to WT cells (Fig. 4, 5). Curve A_m (25°C) refers to the PA signal observed at 25°C with continuous saturating background light, which is the pure thermal expansion signal. Curve A_0 (4°C) is the PA signal produced under weak measuring pulsed light at 4°C, which, theoretically is the pure electrostriction signal. Curve A_0 (25°C) is the combined PA signal generated under weak pulse background light at 25°C. The electrostriction effect is dominant over the thermal expansion in PSII-deficient mutants (Fig. 5a, b). In contrast, the thermal expansion is dominant over electrostriction in PSI-deficient mutants (Fig. 5c, d), indicating that PSII is a major site for photochemical heat dissipation. Similar to the PSII-deficient mutants, a negative (contractive) PA signal was observed in the microsecond time window from the competent RCs in intact cells with open centers, even at room temperature (Fig. 4, curve 3), which implies that the volume contraction of PSI is larger than that of PSII. The PA signals of PSI-deficient mutants were dominant with the volume contraction at 4°C, but thermal expansion at 25°C.

ES efficiencies of PSII and PSI

Analysis of PA signals requires a correction for any fluorescence emission, prompt heat loss, and immediate heat release when the incident energy is beyond the trap energy (Cha and Mauzerall 1992; Malkin and Canaani 1994). These corrections are often negligible. The heat diffusion in the cell matrix allows it to thermally expand until it is cooled by the bulk medium. Thus, this heterogeneous artifact depends on the cell size (Boichenko et al. 2001). We used Eq. 8 in Boichenko et al. (2001) to correct for the "artifact" and calculate the ES_m:

$$ES_m = \frac{PA_m - PA_o}{PA_m} = 1 - \frac{PA_o}{PA_m} \quad (1)$$

$$\frac{PA_o}{PA_m} = \frac{PA_o(25) - PA_o(4)}{PA_m(25) - PA_m(4)}. \quad (2)$$

Here, ES_m is the maximum ES efficiency instead of the maximum ES in the sample; PA_m is the amplitude of PA signal produced when all RCs are closed and the vast majority of absorbed energy (~95%) is dissipated as heat. Under this condition, the PA signal is maximal with a

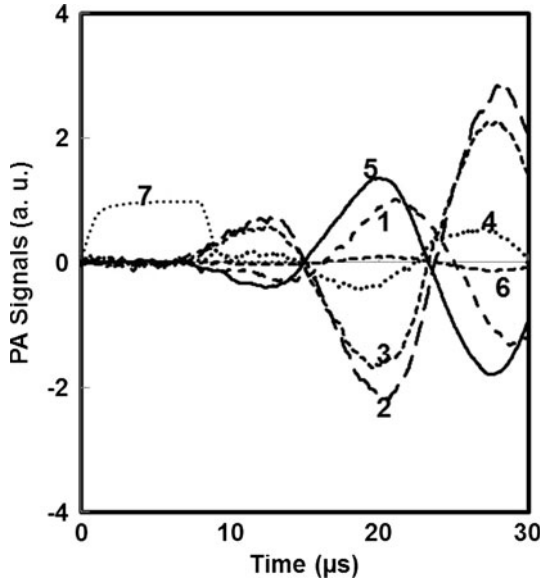

Fig. 4 Photoacoustic profiles of *C. reinhardtii* wild type cell. *Curve 1* 25°C, closed RCs, saturating background light; *curve 2* open RCs, 4°C; *curve 3*, open RCs, 25°C; *curve 4* closed RCs, 4°C; *curve 5* black ink solution, 25°C; *curve 6* black ink solution, 4°C; *curve 7* optical excitation pulse of 8 μs duration

positive phase and serves as an internal calorimetric reference (Callis et al. 1972; Lasser-Ross et al. 1980); PA_o is the amplitude of PA signal generated by a weak light pulse. All the RCs are open for photochemical reaction; therefore the ES is maximal. $PA_o(25)$ refers to the amplitude of PA signal generated under weak pulse light at 25°C (Fig. 4, curve 3), which is the combined PA signal due to both contraction volume change, thermal expansion, and cellular "artifact"; $PA_o(4)$ is the amplitude of PA signal produced under weak pulse light at 4°C (Fig. 4, curve 2), which is attributed to the volume contraction and cellular "artifact"; $PA_m(25)$ is the amplitude of PA signal generated under continuous saturating background light at 25°C (Fig. 4, curve 1), caused by thermal expansion and cellular "artifact"; $PA_m(4)$ is the amplitude of PA signal generated under continuous saturating background light at 4°C (Fig. 4, curve 4), which is the signal produced by the cellular "artifact". Due to low signal-to-noise ratio, we smoothed the PA data and normalized them according to Eq. 2. The PA_o and PA_m signal profiles of different types of cells are summarized in Fig. 6. We noticed that the PA signal from the cell artifact (Fig. 4, curve 4) was relatively

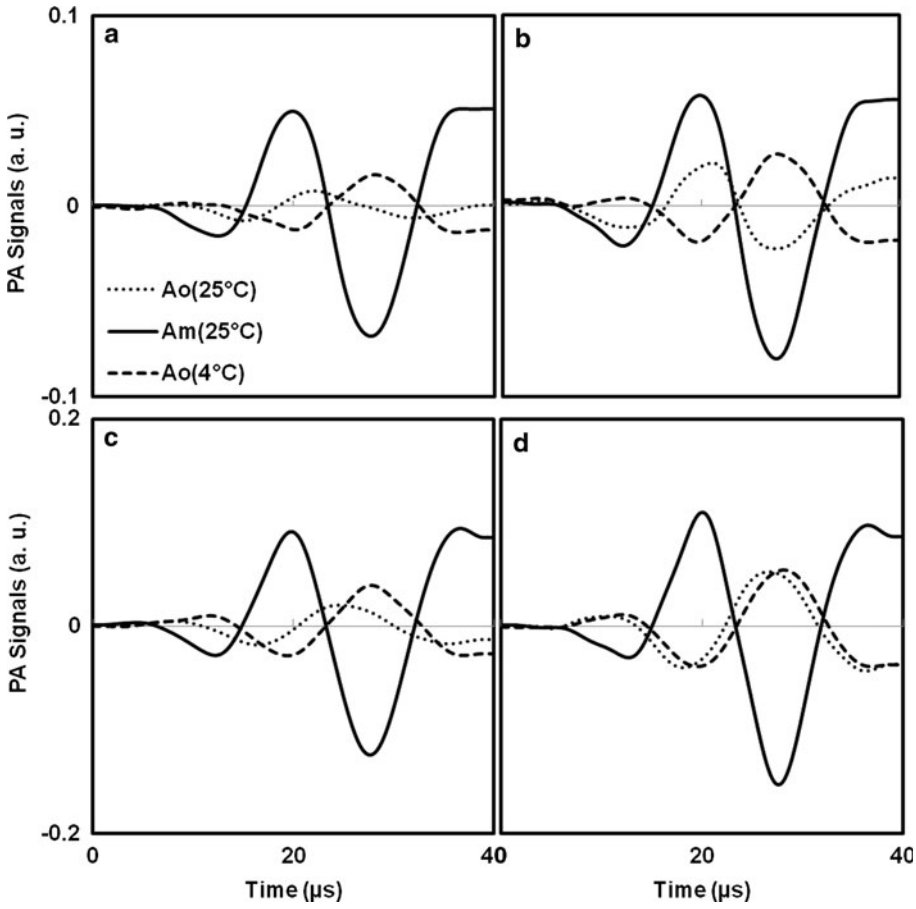

Fig. 5 Photoacoustic profiles corrected for cell "artifacts" **a** CC-4134 and **b** CC-1042 (PSI-deficient mutants); **c** CC-4151 and **d** CC-1051 (PSII-deficient mutants). *Curve* A_0 (25°C), weak pulsed light at 25°C; *curve* A_m (25°C), saturation continuous background light at 25°C; *curve* A_0 (4°C), weak pulsed light at 4°C; all the data were smoothed using the Savitzky–Golay filter in the Origin 6.0 program

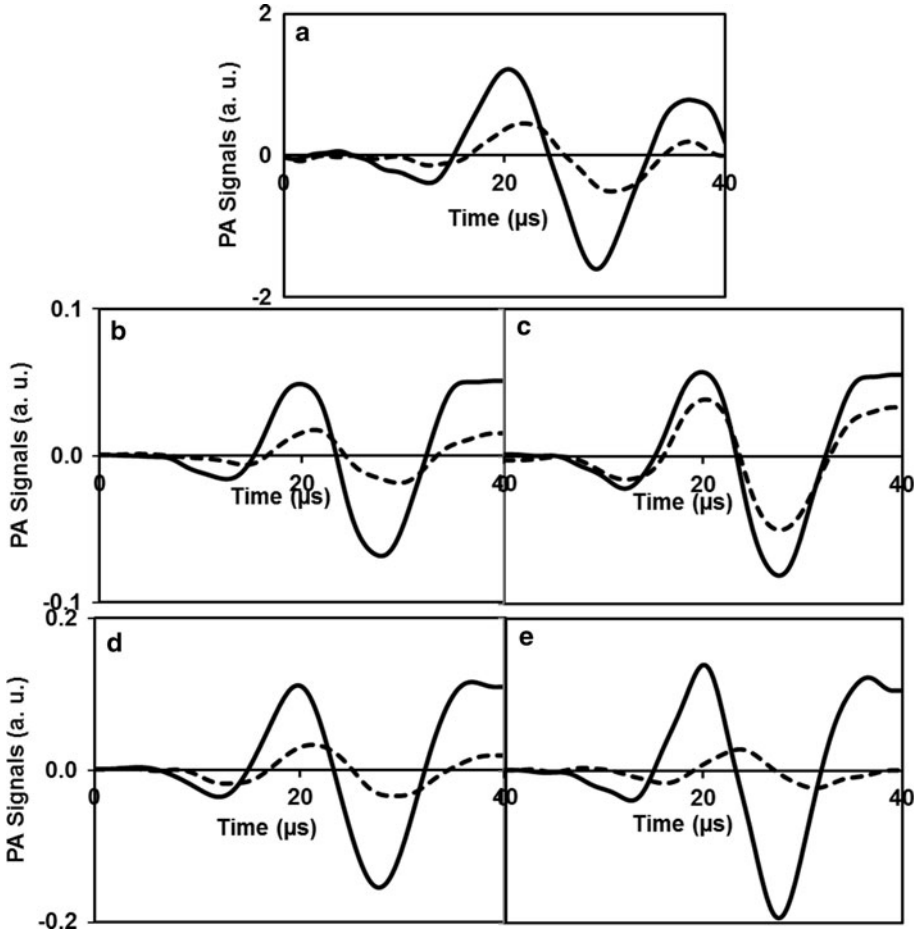

Fig. 6 Corrected PA_o and PA_m spectra. **a** WT; **b** CC-4134 (PSI-deficient mutant); **c** CC-1042 (PSI-deficient mutant); **d** CC-4151 (PSII-deficient mutant); **e** CC-1051 (PSII-deficient mutant). *Solid line* PA_m; *dotted line* PA_o. All data were normalized according to Eq. 2

weak, as expected for large cells (Boichenko et al. 2001). Combining Eqs. 1 and 2, the real ES can be calculated as:

$$ES_m = 1 - \frac{PA_o(25) - PA_o(4)}{PA_m(25) - PA_m(4)}. \quad (3)$$

PA_o and PA_m were determined as the amplitude of its first corresponding PA waveforms recorded at 20 μs (see Fig. 4). In essence, PA_o and PA_m are the magnitudes of the oscillations recorded by a resonance-based PA detector. Based on Eq. 3, we obtained ES efficiencies per on the microsecond time scale as following: $ES_{WT} = 67 \pm 2\%$; $ES_{CC\text{-}4134} = 63\%$; $ES_{CC\text{-}1042} = 37\%$; $ES_{CC\text{-}4151} = 75\%$; $ES_{CC\text{-}0151} = 85\%$; or 67 ± 2, 80 ± 5, and $50 \pm 13\%$ per trap in WT, PSI, and PSII, respectively. As shown in Fig. 7, the ES efficiencies are increasing along the gradient of the PSI content in all four mutants, implying the dependence of the ES efficiencies on PSI content in the algal mutants.

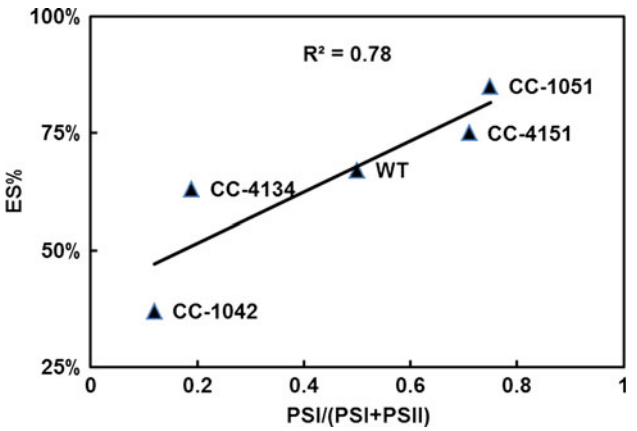

Fig. 7 The relationship between energy storage efficiency (ES%) and PSI/(PSI + PSII) ratios of *C. reinhardtii* WT and mutants. The *solid line* is the least curve fit

Discussion

Generally, long-wavelength fluorescence emissions at 77 K of vascular plants, red algae, green algae, and cyanobacteria are composed of three major fluorescence bands, F_{685}, F_{695}, and $F_{710–735}$ (Murata et al. 1966). The origin of each fluorescence band has been assigned based on their specific action spectra (Murata et al. 1966) obtained from the PSI and PSII complexes (Satoh 1980), and from PSI- or PSII-deficient mutants of cyanobacteria

(Nilsson et al. 1992; Shen and Vermaas 1994). Our 77 K spectral fluorescence measurements confirmed that both CC-4134 and CC-1042 are deficient in the PSI core complex, while CC-4151 and CC-1051 are deficient in PSII.

The variability in PSI/PSII ratio was reflected in the PA signals. The PA profiles of PSI-deficient mutants with open RCs had a positive phase at 25°C, but a negative phase at 4°C (Fig. 5a, b, respectively), which suggests that at room temperature the PA signal is dominated by thermal expansion. In contrast, PSII-deficient mutants showed a large negative amplitude at 25°C and an even larger effect at 4°C (Fig. 5c, d), which strongly suggests that the PA signal in these cells is dominated by volume contraction of the RCs. Further, PSII-deficient mutants exhibited negative signals even at room temperature, suggesting that the thermal losses in PSII are greater than in PSI. This difference reflects the difference in the change in enthalpy of the two photosystems. The enthalpy and volume changes in PSI are similar to those in bacterial RCs of *Rhodopseudomonas sphaeroides* (Edens et al. 2000). The same is supposed to be true for PSII, since the structure and organization of PSII are assumed to be similar to that of bacterial RCs (Trebst 1986; Michel and Deisenhofer 1988; Lancaster et al. 2000; Zouni et al. 2001). However, the PA measurements clearly suggest that the energy migration and photochemical processes in PSII exhibit significantly lower ES efficiency. These results indicate that PSI contributes more to the ES than PSII in photochemical reactions at $\sim$10 μs, which is consistent with previous studies on intact cyanobacteria (Boichenko et al. 2001) and isolated PSI and PSII complexes (Hou et al. 2001a, b).

The volume contraction of PSI RCs reflects the formation of the radical pair $P_{700}{}^{+}F_A/F_B^{-}$ in the microsecond time window (Nugent 1996; Golbeck 1994; Brettel 1997; Diner and Babcock 1996; Hou et al. 2001a). Similar to the bacterial RCs (Yeates et al. 1987), there are excess charges (+13) on the A_1 side and (−1) on the P_{700} side of the membranes, respectively, which could facilitate the transmembrane electron transfer (Hou et al. 2001b). The electrostriction caused by the pure electron-transfer process could induce great volume contraction in PSI, as evident from Fig. 5c, d. The volume contraction of PSI RCs reflects the formation of the radical pair $P_{700}{}^{+}FA/FB^{-}$ in the microsecond time window (Nugent 1996; Golbeck 1994; Brettel 1997; Diner and Babcock 1996; Hou et al. 2001a). Similar to the bacterial RCs (Yeates et al. 1987), there are excess charges (+13) on the A_1 side and (−1) on the P_{700} side of the membranes, respectively, which could facilitate the transmembrane electron transfer (Hou et al. 2001b). The electrostriction caused by the pure electron-transfer process could induce great volume contraction in PSI, as evident from Fig. 5c, d. In contrast, a smaller volume contraction is observed in PSII (Fig. 5a, b). PSII contains a donor tyrosine residue, D1-Tyr-161 (Y_Z), which is absent in bacterial and PSI RCs. If Y_Z is deprotonated before its oxidation by $P_{680}{}^{+}$ (Tommos and Babcock 2000; Diner 2001), the electron transfer from Y_Z^{-} to $P_{680}{}^{+}$ would form $Y_Z{}^{*}Q_A^{-}$. Therefore, the volume contraction in PSII would be relatively small, only differed by the radii of Q_A and Y_Z (Mauzerall et al. 2002). If the deprotonation takes place after the formation of $P_{680}{}^{+}$, we ascribe the small volume contraction in PSII to a rapid proton transfer from oxidized Y_Z to a polar region. The electric field of $P_{680}{}^{+}$ could increase the acidity of the protonated histidine that is close to Y_Z, causing a rapid proton transfer to a polar region while leaving Y_ZH unoxidized, thus the charge would be neutralized with very small electrostriction (Hou et al. 2001a, Mauzerall et al. 2002). The volume contraction was estimated to be about -9 Å^3 by forming $Y_ZP_{680}{}^{+}Q_A^{-}$ and -3 Å^3 by forming $Y_Z{}^{*}Q_A^{-}$ in PSII complex (Hou et al. 2001a; Mauzerall et al. 2002), in contrast to -26 Å^3 by forming $P_{700}{}^{+}F_A/F_B^{-}$ in PSI complex (Hou et al. 2001b).

The ES efficiency depends on the early steps of electron transport within the RCs. In the microsecond time window, separated charges should be stabilized mainly in states $Y_Z{}^{*}P_{680}Q_A^{-}$ for PSII and $P_{700}{}^{+}F_A/F_B^{-}$ for PSI or Fd^{-} in the whole cells (Golbeck 1994; Nugent 1996; Brettel 1997; Diner and Babcock 1996; Hou et al. 2001b; Santabarbara et al. 2010). Contrary to previous interpretations, but in agreement with Hou et al. (2001a, b), our results show that PSI-deficient mutants have lower ES efficiency ($\sim$50%) than PSII-deficient mutants ($\sim$80%). This phenomenon could be due to higher energy losses in the PSII core antenna than in PSI (Delosme et al. 1994). It should be noted that the photoacoustically measured ES efficiency within a certain time scale is an important parameter in defining the electron transport steps under observation. For example, about 40% of electrons are transferred from the RC to photoacoustically silent acceptors in PSII on the millisecond time scale (Cha and Mauzerall 1992; Charlebois and Mauzerall 1999). Nonetheless, it is clear that the inherently low ES efficiency in PSII is a consequence of a shallow excitonic trap, which although capable of oxidizing water, was appropriated from bacterial photosynthetic RCs and is not capable of reducing NADPH without a second photosystem. The inefficiency of PSII clearly means that non-radiative energy dissipation is inherently large in this RC.

In this study, we used intact cells and mutants to measure the PSI and PSII ES in vivo, instead of the commonly used invasive methods in the previous studies, such as extracting the PSI or PSII particles in vitro (Boichenko et al. 2001; Hou et al. 2001a, b), using specific wavelength excitation light to isolate a specific photosystem (Boichenko et al. 2001; Hou et al. 2001a, b; Herbert et al.

2000), or inhibitors (e.g., DCMU) (Cha and Mauzerall 1992). Our measurements revealed that the ES efficiency in *C. reinhardtii* mutants is positively correlated with the ratio of PSI to PSI + PSII. Also, we demonstrated the utility and convenience of the novel PA instrument using simple LEDs instead of complex lasers in measuring the photosynthetic ES efficiency. Moreover, the PA-derived electrostriction characteristics can be applied as an internal reference for the dielectric coefficient of the protein in the RCs and local compressibility of the medium (Mauzerall et al. 1995a, b; Edens et al. 2000). The PA technique offers new opportunities to understand the reaction dynamics of many photochemically active proteins (McClean et al. 1998), by developing a microphotoacoustic spectrometer for the study of protein dynamics (Herbert et al. 2000).

Acknowledgments This study was supported by the US Department of Defense via Strategic Environmental Research and Development Program, NASA, and US-Israel Bi-national Science Foundation, and Rutgers Graduate Fellowship (to CY). We appreciate two anonymous reviewers for their constructive comments.

References

Arata H, Parson WW (1981) Enthalpy and volume changes accompanying electron transfer from P-870 to quinones in *Rhodopseudomonas sphaeroides* reaction centers. Biochim Biophys Acta 636:70–81. doi:10.1016/0005-2728(81)90077-3

Bell AG (1880) On the production and reproduction of sound by light: the photophone. Am J Sci 20:305–324

Boichenko VA, Hou JM, Mauzerall DC (2001) Thermodynamics of electron transfer in oxygenic photosynthetic reaction centers: volume change, enthalpy, and entropy of electron-transfer reactions in the intact cells of the cyanobacterium Synechocystis PCC 6803. Biochemistry 40:7126–7132. doi:10.1021/bi010374k

Borsarelli C, Braslavsky SE (1998) Volume changes correlate with enthalpy changes during the photoinduced formation of the ^{3}MLCT state of ruthenium(II) bipyridine cyano complexes in the presence of salts. A case of the entropy–enthalpy compensation effect. J Phys Chem B 102:6231–6238. doi:10.1021/jp981235o

Borsarelli C, Braslavsky SE (1999) Enthalpy, volume, and entropy changes associated with the electron transfer reaction between the ^{3}MLCT state of $Ru(Bpy)_3^{2+}$ and methyl viologen cation in aqueous solutions. J Phys Chem A 103:1719–1727. doi:10.1021/jp984201

Braslavsky SE, Heibel GE (1992) Time-resolved photothermal and photoacoustic methods applied to photoinduced processes in solution. Chem Rev 92:1381–1410. doi:10.1021/cr00014a007

Brettel K (1997) Electron transfer and redox-cofactors in photosystem I. Biochim Biophys Acta 1318:322–373

Bruce D, Salehian O (1992) Laser-induced optoacoustic calorimetry of cyanobacteria. The efficiency of primary photosynthetic processes on state 1 and state 2. Biochim Biophys Acta Bioenerg 1100:242–250. doi:10.1016/0167-4838(92)90478-V

Brumfeld V, Nagyt L, Kiss V, Malkin S (1999) Wide-frequency hydrophone detection of laser-induced photoacoustic signals in photosynthesis. Photochem Photobiol 70:607–615. doi:10.1111/j.1751-1097.1999.tb08259.x

Cahen D, Malkin S, Lerner EI (1978) Photoacoustic spectroscopy of chloroplast membranes: listening to photosynthesis. FEBS Lett 91:339–342

Callis JB, Parson WW, Goutermann MM (1972) Fast changes of enthalpy and volume on flash excitation of chromatium chromatophores. Biochim Biophys Acta 267:348–362. doi:10.1016/0005-2728(72)90122-3

Canaani O, Malkin S, Mauzerall D (1988) Pulsed photoacoustic detection of flash-induced oxygen evolution from intact leaves and its oscillations. Proc Natl Acad Sci USA 85:4725–4729

Cha Y, Mauzerall DC (1992) Energy storage of linear and cyclic electron flows in photosynthesis. Plant Physiol 100:1869–1877. doi:10.1104/pp.100.4.1869

Charlebois DO, Mauzerall DC (1999) Energy storage and optical cross-section of PSI in the cyanobacterium Synechococcus PCC 7002 and a psaE$^-$ mutant. Photosynth Res 59:27–38. doi:10.1023/A:1006199618668

Delosme R (1998) Wavelength dependence of the quantum yield of charge separation in photosynthesis: photoacoustic study of light energy distribution among various pigment complexes. Israel J Chem 38:237–246

Delosme R (2003) On some aspects of photosynthesis revealed by photoacoustic studies: a critical evaluation. Photosynth Res 76:289–301. doi:10.1023/A:1024977623828

Delosme R, Béal D, Joliot P (1994) Photoacoustic detection of flash-induced charge separation in photosynthetic systems: spectral dependence of the quantum yield. Biochim Biophys Acta Bioenerg 11:56–64. doi:10.1016/0005-2728(94)90193-7

Diner BA (2001) Amino acid residues involved in the coordination and assembly of the manganese cluster of photosystem II. Proton-coupled electron transport of the redox-active tyrosines and its relationship to water oxidation. Biochim Biophys Acta 1503:147–163. doi:10.1016/S0005-2728(00)00220-6

Diner BA, Babcock GT (1996) Structure, dynamics, and energy conversion efficiency in photosystem II. In: Ort DR, Yocum CF (eds) Oxygenic photosynthesis: the light reactions. Kluwer Academic Publishers, Dordrecht, pp 213–247

Edens GJ, Gunner MR, Xu G, Mauzerall DC (2000) The enthalpy and entropy of reaction for formation of P+ QA− from excited reaction centers of *Rhodobacter sphaeroides*. J Am Chem Soc 122:1479–1485. doi:10.1021/ja991791b

Feitelson J, Mauzerall DC (1993) Wide band time resolved photoacoustic study of electron transfer reactions: difference between measured enthalpy and redox free energies. J Phys Chem 97:8410–8413. doi:10.1021/j100004a00

Fork DC, Herbert SK (1993) The application of photoacoustic techniques to studies of photosynthesis. Photochem Photobiol 57:207–220. doi:10.1111/j.1751-1097.1993.tb02277.x

Golbeck JH (1994) Photosystem I in cyanobacteria. In: Bryant DA (ed) The molecular biology of cyanobacteria. Kluwer Academic Publishers, Dordrecht, pp 319–360

Herbert SK, Han T, Vogelmann TC (2000) New applications of photoacoustics to the study of photosynthesis. Photosynth Res 66:13–31. doi:10.1023/A:1010788504886

Hou JM, Boichenko VA, Diner BA, Mauzerall DC (2001a) Thermodynamics of electron transfer in oxygenic photosynthetic reaction centers: volume change, enthalpy, and entropy of electron-transfer reactions in manganese-depleted photosystem II core complexes. Biochemistry 40:7117–7125. doi:10.1021/bi010373s

Hou JM, Boichenko VA, Wang YC, Chitnis PR, Mauzerall DC (2001b) Thermodynamics of electron transfer in oxygenic photosynthetic reaction centers: a pulsed photoacoustic study of electron transfer in photosystem I reveals a similarity to bacterial reaction centers in both volume change and entropy. Biochemistry 40:7109–7116. doi:10.1021/bi0103720

Kolbowski J, Reising H, Schreiber U (1990) Computer controlled pulse modulation system for analysis of photoacoustic signals in the time domain. Photosynth Res 25:309–316. doi:10.1007/BF00033172

Krause GH, Weis E (1991) Chlorophyll fluorescence and photosynthesis: the basics. Annu Rev Plant Physiol Plant Mol Biol 42:313–349. doi:10.1146/annurev.pp.42.060191.001525

Lancaster CRD, Bibikova MV, Sabatino P, Oesterhelt D, Michel H (2000) Structural basis of the drastically increased initial electron transfer rate in the reaction center from a *Rhodopseudomonas viridis* mutant described at 2.00-Å resolution. J Biol Chem 275:39364–39368. doi:10.1074/jbc.M008225200

Lasser-Ross N, Malkin S, Cahen D (1980) Photoacoustic detection of photosynthetic activities in isolated broken chloroplasts. Biochim Biophys Acta 593:330–341. doi:10.1016/0005-2728(80)90070-5

Losi A, Braslavsky SE, Gartner W, Spudich JL (1999) Time-resolved absorption and photothermal measurements with sensory rhodopsin I from *Halobacterium salinarum*. Biophys J 76:2183–2191. doi:10.1016/S0006-3495(99)77373-X

Malkin S (1996) The photoacoustic method in photosynthesis-monitoring and analysis of phenomena which lead to pressure changes following light excitation. In: Amesz J, Hoff A (eds) Biophysical techniques in photosynthesis. Kluwer Academic Publishers, Dordrecht, pp 191–206

Malkin S, Cahen D (1979) Photoacoustic spectroscopy and radiant energy conversion: theory of the effect with special emphasis on photosynthesis. Photochem Photobiol 29:803–813. doi:10.1111/j.1751-1097.1979.tb07770.x

Malkin S, Canaani O (1994) The use and characteristics of the photoacoustic method in the study of photosynthesis. Annu Rev Plant Physiol Plant Mol Biol 45:493–526. doi:10.1146/annurev.pp.45.060194.002425

Mauzerall DC (1990) Determination of oxygen emission and uptake by pulsed, time resolved photoacoustics. Plant Physiol 94:278–283. doi:10.1104/pp.94.1.278

Mauzerall DC, Feitelson J, Prince R (1995a) Wide band, time-resolved photoacoustic study of electron transfer reactions: difference between measured enthalpies and redox free energies. J Phys Chem 99:1090–1093. doi:10.1021/j100004a006

Mauzerall DC, Gunner MR, Zhang JW (1995b) Volume contraction on photoexcitation of the reaction center from *Rhodobacter sphaeroides* R-26: internal probe of dielectrics. Biophys J 68:275–280. doi:10.1016/S0006-3495(95)80185-2

Mauzerall DC, Feitelson J, Dubinsky Z (1998) Discriminating between phytoplankton taxa by photoacoustics. Israel J Chem 38:257–260

Mauzerall DC, Hou JM, Boichenko V (2002) Volume changes and electrostriction in the primary photoreactions of various photosynthetic systems: estimation of dielectric coefficient in bacterial reaction centers and of the observed volume changes with the Drude–Nernst equation. Photosynth Res 74:173–180. doi:10.1023/A:1020903525973

McClean MA, Di Primo C, Deprez E, Hoa GHB, Sligar SG (1998) Photoacoustic calorimetry of proteins. Methods Enzymol 295:316–330

Michel H, Deisenhofer J (1988) Relevance of the photosynthetic reaction center from purple bacteria to the structure of photosystem II. Biochemistry 27:1–7. doi:10.1021/bi00401a001

Mimuro M, Murakami A, Fujita Y (1982) Studies on spectral characteristics of allophycocyanin isolated from *Anabaena cylindrica*: curve-fitting analysis. Arch Biochem Biophys 215:266–273. doi:10.1016/0003-9861(82)90304-6

Mullineaux CW, Griebenow S, Braslavsky SE (1991) Photosynthetic energy storage in cyanobacterial cells adapted to light-states 1 and 2. A laser-induced optoacoustic study. Biochim Biophys Acta 1060:315–318. doi:10.1016/S0005-2728(05)80323-8

Murakami A (1997) Quantitative analysis of 77 K fluorescence emission spectra in *Synechocystis* sp. PCC 6714 and *Chlamydomonas reinhardtii* with variable PS I/PS II stoichiometries. Photosynth Res 53:141–148. doi:10.1023/A:1005818317797

Murakami A, Fujital Y, Nemson JA, Melis A (1997) Chromatic regulation in *Chlamydomonas reinhardtii*: time course of photosystem stoichiometry adjustment following a shift in growth light quality. Plant Cell Physiol 38:188–193

Murata N, Nishimura M, Takamiya A (1966) Fluorescence of chlorophyll in photosynthetic systems. III. Emission and action spectra of fluorescence—three emission bands of chlorophyll a and the energy transfer between two pigment systems. Biochim Biophys Acta 126:234–243. doi:10.1016/0926-6585(66)90059-8

Nilsson F, Simpson DJ, Jansson C, Andersson B (1992) Ultrastructural and biochemical characterization of a Synechocystis 6803 mutant with inactivated psbA genes. Arch Biochim Biophys 295:340–347. doi:10.1016/0003-9861(92)90526-3

Nitsch C, Braslavsky SE, Schatz GH (1988) Laser-induced calorimetry of primary processes in isolated photosystem I and photosystem II particles. Biochim Biophys Acta 934:201–212. doi:10.1016/0005-2728(88)90183-1

Nugent JHA (1996) Oxygenic photosynthesis: electron transfer in photosystem I and photosystem II. Eur J Biochem 237:519–531. doi:10.1111/j.1432-1033.1996.00519.x

Paltauf G, Nuster R, Haltmeier M, Burgholzer P (2007) Photoacoustic tomography using a Mach Zehnder interferometer as an acoustic line detector. Appl Opt 46:3352–3358. doi:10.1364/AO.46.003352

Polle JEW, Benemann JR, Tanaka A, Melis A (2000) Photosynthetic apparatus organization and function in wild type and a Chl b-less mutant of Chlamydomonas reinhardtii. Dependence on carbon source. Planta 211(3):335–344. doi:10.1007/s004250000279

Santabarbara S, Galuppini L, Casazza AP (2010) Bidirectional electron transfer in the reaction centre of photosystem I. J Integr Plant Biol 52:735–749. doi:10.1111/j.1744-7909.2010.00977.x

Satoh K (1980) F-695 emission from the purified photosystem II chlorophyll a-protein complex. FEBS Lett 110:53–56

Shen G, Vermaas WFJ (1994) Chlorophyll in a *Synechocystis* sp. PCC 6803 mutant without photosystem I and photosystem II core complexes. Evidence for peripheral antenna chlorophylls in cyanobacteria. J Biol Chem 269:13904–13910

Sueoka N (1960) Mitotic replication of deoxyribonucleic acid in *Chlamydomonas reinhardtii*. Proc Natl Acad Sci USA 46:83–91

Tommos C, Babcock GT (2000) Proton and hydrogen currents in photosynthetic water oxidation. Biochim Biophys Acta 1458:199–219. doi:10.1016/S0005-2728(00)00069-4

Trebst A (1986) The topology of the plastoquinone and herbicide binding peptides of photosystem II in the thylakoid membrane. Z Naturforsch 41c:240–245

Wegewijs B, Paddon-Row MN, Braslavsky SE (1998) Volume change associated with large photoinduced dipole formation in a rigid donor–acceptor compound: new approach to optoacoustic volume determination. J Phys Chem A 102:8812–8818. doi:10.1021/jp982751h

Xu M, Wang LV (2006) Photoacoustic imaging in biomedicine. Rev Sci Instrum 77:041101-1–22. doi:10.1063/1.2195024

Yeates TO, Komiya H, Rees DC, Allen JP, Feher G (1987) Structure of the reaction center from *Rhodobacter sphaeroides* R-26: the cofactors. Proc Natl Acad Sci USA 84:6438–6442

Zouni A, Witt HT, Kern J, Fromme P, Norbert Krauss N, Saenger W, Orth P (2001) Crystal structure of photosystem II from *Synechococcus elongatus* at 38 Å resolution. Nature 409:739–743. doi:10.1038/35055589